Self-Assembled Colloidal Arrays as Three-Dimensional Nanofluidic Sieves for Separation of Biomolecules on Microchips

ARTICLE *in* ANALYTICAL CHEMISTRY · APRIL 2007

Impact Factor: 5.64 · DOI: 10.1021/ac061931h · Source: PubMed

Self-Assembled Colloidal Arrays as Three-Dimensional Nanofluidic Sieves for Separation of Biomolecules on Microchips

Yong Zeng and D. Jed Harrison*

Department of Chemistry, University of Alberta, Edmonton AB, T6G 2G2, Canada

We report on a biomolecular sieving system based on the use of ordered colloidal arrays to define the sieve structure within a microfluidic device. A facile microfluidic colloidal self-assembly strategy has been developed to create ordered, robust, three-dimensional nanofluidic sieves within microfluidic devices, with which fast separation of DNA and proteins of a wide size range was achieved. Compared to conventional colloidal deposition procedures, such as vertical deposition, this approach features much faster assembling speed, the absence of drying-caused cracks that may jeopardize the separation performance, and better flexibility to couple with current microfabrication techniques. The flexibility of pore size enabled by this methodology provides separation of biomolecules with a wide size distribution, ranging from proteins (20−200 kDa) to dsDNA (0.05−50 kbp). Under moderate electric fields, complete separation can be finished in minutes, with separation efficiency comparable to gel/polymer-filled or micro-/nanofabricated microsystems. To our knowledge, this is the first demonstration of size separation of biomolecules within self-assembled ordered colloidal lattices embedded within a microfluidic system.

Size-based separation techniques have been the popular workhorse for sample preparation and analysis in genomics, proteomics, and molecular biology. Compared with conventional slab gel-based electrophoretic techniques, miniaturized systems offer many advantages in terms of higher separation speed, minute consumption of reagents, and integration of multiple functions. Most separation microsystems, however, still rely on gels or polymer solutions for separation of nucleic acids[1] and proteins.[2,3] Recently, micro-/nanofabricated molecule-sorting structures have received great interest since they provide means to improve the efficiency and speed of biomolecular separation.[4] A variety of micro-/nanomachined sieves have been designed for separating biomolecules[5−14] and particles.[14] Compared with conventional gels and polymer matrixes, artificial gel structures feature regular and precisely engineered geometry, mechanical robustness, and easy integration. The well-characterized topologies of micro-/nanofabricated structures make deliberate modifications of molecular transport possible, catalyzing the exploration of new mechanisms for size-based fractionation, such as entropic trapping,[15] entropic recoil,[16] Brownian ratchets,[10] and laminar flow bifurcation.[14] However, most micro-/nanomachined structures were designed for large DNA molecules, generally due to technical challenges in lithographically accessing structures on the dimensions of smaller molecules, such as proteins (<∼10 nm). Conventional micro-/nanofabrication techniques also suffer from some disadvantages, such as requiring sophisticated facilities and time-consuming procedures, and normally producing 2D architectures, which impedes their applications on a routine base.

Spontaneous organization of monodisperse, micro- and nanometer-sized particles, referred to as colloidal self-assembly (CSA), provides a simple and cost-effective alternative to conventional techniques for creating three-dimensional, periodic nanostructures. Applications of CSA include material synthesis,[17] photonic band gap crystals,[18] and biological and chemical sensors.[19] Recently, self-assembled colloidal crystals have attracted interest in the fields of separation and polymer dynamics, owing

* To whom correspondence should be addressed. E-mail: jed.harrison@ualberta.ca.

(1) Kan, C. W.; Fredlake, C. P.; Doherty, E. A. S.; Barron, A. E. *Electrophoresis* **2004**, *25*, 3564−3588.
(2) Yao, S.; Anex, D. S.; Caldwell, W. B.; Arnold, D. W.; Smith, K. B.; Schultz, P. G. *Proc. Natl. Acad. Sci. U.S.A.* **1999**, *96*, 5372−5377.
(3) Herr, A. E.; Singh, A. K. *Anal. Chem.* **2004**, *76*, 4727−4733.
(4) Lin, Y. W.; Huang, M. F.; Chang, H. T. *Electrophoresis* **2005**, *26*, 320−330.
(5) Volkmuth, W. D.; Austin, R. H. *Nature* **1992**, *358*, 600−602.
(6) Han, J.; Craighead, H. G. *Science* **2000**, *288*, 1026−1029.
(7) Han, J.; Craighead, H. G. *Anal. Chem.* **2002**, *74*, 394−401.
(8) Cabodi, M.; Turner, S. W.; Craighead, H. G. *Anal. Chem.* **2002**, *74*, 5169−5174.
(9) Cabodi, M.; Chen, Y. F.; Turner, S. W. P.; Craighead, H. G.; Austin, R. H. *Electrophoresis* **2002**, *23*, 3496−3503.
(10) Chou, C. F.; Bakajin, O.; Turner, S. W. P.; Duke, T. A. J.; Chan, S. S.; Cox, E. C.; Craighead, H. G.; Austin, R. H. *Proc. Natl. Acad. Sci. U.S.A.* **1999**, *96*, 13762−13765.
(11) Huang, L. R.; Tegenfeldt, J. O.; Kraeft, J. J.; Sturm, J. C.; Austin, R. H.; Cox, E. C. *Nat. Biotechnol.* **2002**, *20*, 1048−1051.
(12) Kaji, N.; Tezuka, Y.; Takamura, Y.; Ueda, M.; Nishimoto, T.; Nakanishi, H.; Horiike, Y.; Baba, Y. *Anal. Chem.* **2004**, *76*, 15−22.
(13) Fu, J.; Mao, P.; Han, J. *Appl. Phys. Lett.* **2005**, *87*, 263902.
(14) Huang, L. R.; Cox, E. C.; Austin, R. H.; Sturm, J. C. *Science* **2004**, *304*, 987−990.
(15) Han, J.; Turner, S. W.; Craighead, H. G. *Phys. Rev. Lett.* **1999**, *83*, 1688−1691.
(16) Turner, S. W. P.; Cabod, M.; Craighead, H. G. *Phys. Rev. Lett.* **2002**, *88*, 1−4.
(17) Velev, O. D.; Lenhoff, A. M. *Curr. Opin. Colloid Interface Sci.* **2000**, *5*, 56−63.
(18) Vlasov, Y. A.; Bo, X.; Sturm, J. C.; Norris, D. J. *Nature* **2001**, *414*, 289−293.
(19) Reese, C. E.; Asher, S. A. *Anal. Chem.* **2003**, *75*, 3915−3918.

to the relatively simple fabrication and the uniquely ordered porous structure. Reversible colloidal pillar arrays self-organized under a magnetic field have been applied to microfluidic separation of long DNA.[20] Self-assembled colloidal lattices have been employed to probe Brownian diffusion[21] and electrophoretic migration[22,23] of confined single biopolymer molecules. Recently, Wirth et al. reported high-speed electrochromatographic separation of fluorescent dyes and peptides inside a silica colloidal stripe prepared by the vertical deposition process.[24] However, the use of a colloidal lattice for size separation of biomolecules has not been reported. In addition, there is still a lack of convenient approaches for high-speed fabrication of crack-free colloidal arrays within microfluidic systems. Conventional techniques, such as gravitational sedimentation[22] and evaporation-based vertical deposition,[23,24] normally demand a period from tens of hours to days to deposit colloidal array into fluidic devices. They also pose challenges in sealing the deposited colloidal lattices to create enclosed microsystems without disturbing their structures. Vertical deposition suffers from the formation of cracks that prevent good separation performance, mainly due to the inevitable drying stress and the shrinkage of beads.[25] Physical confinements, such as microcapillaries[26,27] and fluidic cells,[28,29] provide an effective way to pattern colloidal crystals within microstructures, but have not been used to fabricate complete analytical microsystems based on colloidal structures.

In this work, we present the first demonstration of gel-free size fractionation of biomolecules within ordered colloidal arrays, which are embedded inside microfluidic channels as a three-dimensional nanofluidic sieving structure. We have established a microfluidic colloidal self-assembly technique that dramatically reduces preparation time and avoids the formation of drying-caused cracks. Using this simple technique, robust colloidal lattices of various pore sizes and materials can be readily incorporated into microfluidic devices for rapid separation of biomolecules with a wide size distribution, such as sodium dodecyl sulfate (SDS)−protein complexes, short and long DNA fragments.

EXPERIMENTAL SECTION

DNA and Protein Samples. All reagents and samples were prepared with deionized water (18.2 MΩ) obtained from an Ultrapure water system (Millipore, Milford, MA). Various DNA samples were used, including bacteriophage λ-DNA and calf thymus DNA (Sigma, St. Louis, MO), 50-bp DNA ladder (Amersham Pharmacia Biotech, Piscataway, NJ), PCR marker (Promega, Madison, WI), and other DNA markers and ladders from Invitrogen. Intercalating fluorescent dye YOYO-1 (Molecular Probes, Eugene, OR) was used to stain DNA samples at the dye-to-base pair ratio of ~1:10 in 4× TBE buffer (356 mM Tris-borate, 8 mM EDTA, pH 8.3) containing 4% v/v 2-mercaptoethanol to reduce photobleaching. Final DNA concentrations were 10−60 ng/μL. For denatured protein separation, trypsin inhibitor (soybean, 20.1 kDa), ovalbumin (chicken egg, 45 kDa), bovine serum albumin (66 kDa), phosphorylase B (rabbit muscle, 97 kDa), β-galactosidase (*Escherichia coli*, 116 kDa), and myosin (rabbit muscle, 205 kDa) (Sigma) were used as molecular weight standards. Proteins were conjugated with Alexa Fluor 488 (Molecular Probes). The concentration of proteins varied from 10^{-6} to 10^{-4} M after labeling. An aliquot of each protein solution was mixed with the same volume sample buffer (4× TBE buffer, 4% w/v SDS, 8% v/v 2-mercaptoethanol) and then incubated at 85 °C for 5 min. After denaturizing, protein samples were diluted with buffer solution (4× TBE buffer, 0.1% w/v SDS) and mixed before separation with the final concentration of each component adjusted to 10^{-8}−10^{-7} M in the mixture.

Microchip Fabrication. PDMS microchips were fabricated using standard soft lithography.[30] A positive photoresist master (AZ-4620, Clariant Corp., Charlotte, NC) was UV patterned on a 4-in. silicon wafer, and the mold was silanized to facilitate removal of PDMS. Negative PDMS replicas were made by pouring a 10:1 mixture of PDMS base (Sylgard 184, Dow Corning, Midland, MI) with the curing agent over the wafer, followed by curing at 60 °C overnight. PDMS replicas were removed from the master and reservoir holes were punched to access channels. All devices were assembled by sealing PDMS replicas to clean glass slides without oxygen plasma oxidization. Unless otherwise specified, microchips with a 100-μm offset double-T injector were used, as sketched in Figure 1A. Channels were ~100 μm wide and ~20 μm deep. The buffer and injection channels were 4 mm long, and the separation channel was 10 mm long.

Microfluidic Colloidal Self-Assembly. Monodisperse plain polystyrene (PS) microspheres (2.62% w/v, 1.53 ± 0.039 μm in diameter) and silica beads (10% w/v, 0.90 ± 0.04 μm in diameter) were obtained from Polysciences (Warrington, PA). Uniform silica beads of 166 and 330 nm in diameter (10% w/v, <10% deviation) were obtained from Bangs Laboratories. These aqueous suspensions were ultrasonicated for 10 min prior to use.

The process of microfluidic colloidal self-assembly is schematically illustrated in Figure 1A. A 10−15-μL colloidal suspension was injected into reservoirs 1, 2, and 3. The aqueous solution fills the channels spontaneously, forming a liquid meniscus at the outlet of the channel in reservoir 4. Once all channels were filled, reservoirs 1, 2, and 3 were covered with a PDMS piece to prevent solvent evaporation. Reservoir 4 was left open so that evaporation induced colloidal growth within the channels. The growth of the colloidal array can be stopped by replacing the colloidal suspension in the reservoirs with water. Before separations, the water in the reservoirs was substituted with the running buffer and the device was left to equilibrate for ~20 min.

Separation and Fluorescence Detection. The 4× TBE buffer was used with silica sphere arrays to reduce electroosmotic flow (EOF), with different additives added: 4% v/v 2-mercaptoethanol (anti-photobleaching agent) for DNA separation and 0.1%

(20) Doyle, P. S.; Bibette, J.; Bancaud, A.; Viovy, J.-L. *Science* **2002**, *295*, 2237.
(21) Nykypanchuk, D.; Strey, H. H.; Hoagland, D. A. *Science* **2002**, *297*, 987−990.
(22) Meistermann, L.; Tinland, B. *Phys. Rev. E* **2000**, *62*, 4014−4017.
(23) Zhang, H.; Wirth, M. J. *Anal. Chem.* **2005**, *77*, 1237−1242.
(24) Zheng, S.; Ross, E.; Legg, M. A.; Wirth, M. J. *J. Am. Chem. Soc.* **2006**, *128*, 9016−9017.
(25) Jiang, P.; Bertone, J. F.; Hwang, K. S.; Colvin, V. L. *Chem. Mater.* **1999**, *11*, 2132−2140.
(26) Moon, J. H.; Kim, S.; Yi, G.; Lee, Y. H.; Yang, S. M. *Langmuir* **2004**, *20*, 2033−2035.
(27) Xia, Y.; Kim, E.; Whitesides, G. M. *J. Am. Chem. Soc.* **1996**, *11*, 9576−9577.
(28) Ishii, M.; Nakamura, H.; Nakano, H.; Tsukigase, A.; Harada, M. *Langmuir* **2005**, *21*, 5367−5371.
(29) Lu, Y.; Yin, Y.; Gates, B.; Xia, Y. *Langmuir* **2001**, *17*, 6344−6350.
(30) Effenhauser, C. S.; Bruin, G. J. M.; Paulus, A.; Ehrat, M. *Anal. Chem.* **1997**, *69*, 3451−3457.

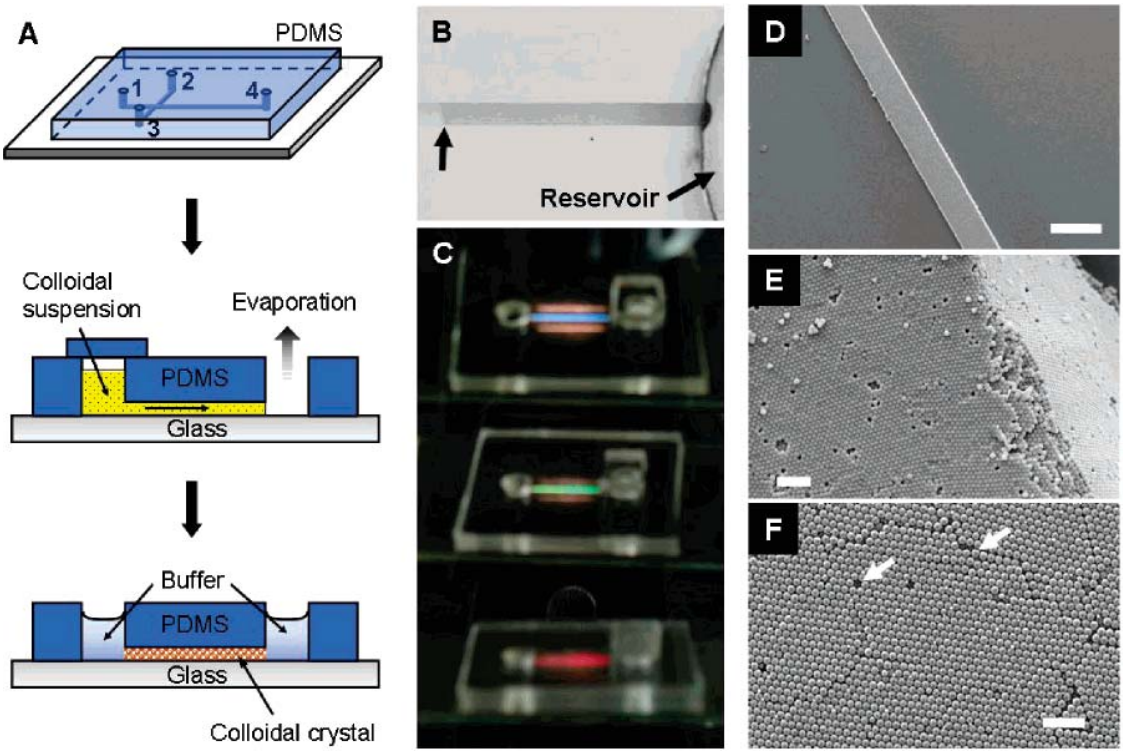

Figure 1. Fabrication and characterization of self-assembled colloidal arrays within microfluidic systems. (A) Schematic illustration of microfluidic colloidal self-assembly in a one-dimensional separation microchip (PDMS chip layout: 1 buffer, 2 sample, 3 sample waster, 4 buffer waste). (B) Optical micrograph of a translucent 0.9-μm silica sphere array growing inside a microchannel (as indicated by the left arrow), showing a convex evaporation interface at the channel opening. (C) Digital images of a PDMS chip packed with 0.9-μm silica spheres before drying. When illuminated by white light vertically from the bottom, the array exhibited monochromic transmitted light at various angles due to Bragg diffraction. (D, E) SEM images of a matrix of 330-nm silica spheres at different magnifications. (F) SEM image of a hexagonally closed packed 2-μm PS colloidal array fabricated within a microchannel. The arrows indicate lattice defects. The scale bars are 200, 2, and 10 μm in (D−F), respectively.

w/v SDS for proteins, respectively. The packed channels were prerun under ~20 V/cm until the current through the channels became static. Samples were loaded from reservoir 2 by applying a 60−80-V potential to reservoir 3 with other reservoirs grounded to form a "pinched" injection plug. Separation was performed under electric fields between 5 and 60 V/cm with a "pull-back" voltage applied to reservoirs 2 and 3 to prevent sample leakage from the loading arms into the separation channel. It was found that salts in the concentrated buffer are easy to precipitate out due to the permeation of water vapor through the PDMS bulk. This issue can be solved by saturating PDMS replicas in water overnight before assembling with glass substrates.

Separation was monitored using epifluorescence microscopy and digital image collection. Samples were excited with an expanded 488-nm argon ion laser beam, and the emission was collected with a high-sensitivity CCD and a homemade inverted microscope equipped with a 505DRLP dichroic mirror, 515-nm-long pass filter, and a 40× planachromat objective (0.6 NA, LDN, Carl Zeiss). Digitized images were stored in a computer and analyzed using ImageJ (NIH, Bethesda, MD, http://rsb.info.nih-.gov/ij/).

Safety Consideration. YOYO-1 intercalating dye is a potential mutagen, and 2-mercaptoethanol is toxic; gloves should be worn when the solutions are handled.

RESULTS AND DISCUSSION

Microfluidic Colloidal Self-Assembly. We performed in situ colloidal crystallization within prefabricated microfluidic separation devices, yielding a simple and rapid route to separation bed formation that is compatible with standard microfabrication processes. The channels were spontaneously filled with an aqueous dispersion of colloids by wetting the hydrophilic glass substrate surface. The flow halted at the edge of the channel outlet in reservoir 4 due to capillary force, forming a convex vapor−liquid interface, as seen in Figure 1B. Evaporation triggers the nucleation of microspheres at the interface and creates a one-directional solvent flow to continuously pack the colloidal beads. The microchannel confinement restricts water evaporation to the channel outlet during the assembling process, so that the packed beds remain wet while packing. In Figure 1B, the translucence of the compact bed of 0.9-μm silica spheres evidence the presence of interstitial water and no invasion of air into the colloidal array. This can be attributed to strong particle surface wetting, which forms nanomenisci between close-packed spheres at the interface.[31] The capillary tension of the nanomenisci creates the enormous negative capillary pressure, estimated to be as low as −300 psi for 0.9-μm silica spheres, which is required to pull water through the porous packed region. As a result, the evaporating interface is fixed within the vicinity of the channel opening. Therefore, in contrast to vertical deposition, this approach prevents drying of the packed bulk during the assembling process, eliminating drying-caused crack formation.

(31) Dufresne, E. R.; Corwin, E. I.; Greenblatt, N. A.; Ashmore, J.; Wang, D. Y.; Dinsmore, A. D.; Cheng, J. X.; Xie, X. S.; Hutchinson, J. W.; Weitz, D. A. *Phys. Rev. Lett.* **2003**, *91*, 224501.

Table 1. Summary of Pore Sizes and Effective Size Ranges for the Colloidal Sieves Constructed with Various Particles

particles with nominal size (nm)	pore size[a] (nm)	effective size range[b] DNA (bp)	effective size range[b] protein (kDa)	equivalent gels[c]
silica, 900	~135	100−2000[d]		2% agarose gel
silica, 330	~50	50−1000	100−205	2−3% agarose or 4 T% polyacrylamide gel
silica, 160	~24		20−205	6 T% polyacrylamide gel

[a] Calculated as ~15% particle sizes. [b] Determined for linear dsDNA and SDS-denatured proteins. [c] Compared according to the targeted size range of separation. [d] Tested to separate long DNA molecules up to ~50 kbp.

Figure 1C demonstrates that a bed of 0.9-μm silica beads packed in a straight channel exhibited monochromic transmitted lights at various specific angles away from normal. This is due to Bragg diffraction, and it indicates the ordered crystalline structure generated within the microchannel. Figure 1D shows a typical SEM image of an array of 330-nm silica particles patterned within a microchannel, which was slowly dried by vapor permeation through the PDMS to minimize the perturbation on the colloidal structure due to drying. No large cracks were observed over the entire structure, while a very low density of small cracks was still present, due mainly to the SEM sample preparation process. A closeup of this bed, shown in Figure 1E, illustrates the close-packed arrangement of the monodisperse colloids and the long-range order over three dimensions. A low density of defects was seen, including point voids, dislocation lines, and stacking faults, as seen in Figure 1E and F. These defects may affect the separation performance. However, they are randomly distributed and localized so that no accumulative effects, such as channeling of flow, will arise.

Our approach offers significantly greater assembly speed than conventional colloidal deposition approaches, which usually take tens of hours to days to construct colloidal arrays within microdevices.[22,28,29] For example, it takes less than 30 min for 10% w/v 0.9-μm silica colloids (~0.4−0.6 mm/min) and less than 60 min for 10% w/v 0.33-μm silica beads to pack a separation channel 1 cm in length under ambient conditions. The high assembly speed can be attributed to the large surface area of the protruding evaporation interface (Figure 1B). Compared to the design of microfabricated barrier structures with a gap size smaller than the particles to be trapped,[29] our approach uses the air−liquid interface as a virtual frit to retain the microspheres, which offers advantages in terms of much larger evaporation area as well as simplified device fabrication. The high-speed assembly allows the packing of large particles of various materials, as exemplified by a regularly packed array of 2-μm PS colloids shown in Figure 1F. Large particles are problematic for slow vertical deposition due to the their relatively rapid sedimentation.[18] The demonstrated ability of our approach to assemble large colloids allows an extended pore size range that can access diverse biomolecules with a wide size range, as shown below.

Size-Based Separation of dsDNA. Nanometer-sized interstices in the close-packed sphere lattice create a nanofluidic sieve that consists of voids interconnected by narrower pores, which have an equivalent diameter ~15% of the sphere size. Molecules experience a loss in entropy by steric constriction while traveling through a constraining pore.[32] Thus, the porous structure imposes periodically modulated free-energy barriers to molecular transport, which is presumably responsible for size-dependent separation of molecules with dimensions comparable to the narrower pore sizes. A variety of self-assembled colloidal sieves were tested; the pore sizes of the lattices are listed in Table 1.

Negative surface charges on particles in a colloidal array cause EOF. Using a high ionic strength buffer is a convenient way to substantially quench this EOF in size-based separation of biopolymers.[6,13] We found 4× TBE quenches EOF sufficiently to be used for all separations in our systems. Figure 2A shows a sequence of fluorescent images of the separation of a low DNA mass ladder at 15 V/cm in a microchip packed with 900-nm silica beads. Six equimolar dsDNA fragments from 100 to 2000 bp were separated into distinct bands within the first 1 mm of the column in ~1.5 min, as seen in the bottom frame of Figure 2A. The 100-bp band was hard to visualize in this low-magnification imaging mode (4× objective) because of its very low concentration. Four consecutive runs of the same ladder were performed in a 0.9-μm silica particle array, and the electropherograms are superimposed in Figure 2B. In this case, the detector was located 5 mm from the injection point. The device was operated for ~5 h before this reproducibility test. The standard deviation of the migration time between these runs is less than 2%, which indicates the stability of the self-assembled colloidal sieve under the applied electric field. The bed stability is likely a result of van de Waals forces between silica particles[23,33] and the contribution from hydrogen bonds between the surfaces of close-packed silica particles. Matrixes composed of silica microspheres of 160, 330, and 900 nm and polystyrene beads of 770 and 1530 nm were found durable under applied fields as high as 60 V/cm. Redispersion of beads away from the packed bed may occur at the exits of the channels, but this is limited to a distance less than 200 μm into the channels. In this proof-of-concept study, no further steps were performed to strengthen the packed beds, as their stability was satisfactory. Further sintering can greatly enhance the adhesion by using additional modifications, such as thermal treatment.[34] However, this simple, rapid method for the preparation of nanofluidic sieve structures for biomolecular separation may not require greater stability, because of the ease of preparing new columns. Easily replaceable columns may also have benefits.

The separation performance in the 0.9-μm colloidal array was further investigated at different electric fields, three of which are

(32) Giddings, J. C. *Unified Separation Science*; Wiley: New York, 1991.
(33) Norris, D. J.; Arlinghaus, E. G.; Meng, L.; Heiny, R.; Scriven, L. E. *Adv. Mater.* **2004**, *16*, 1393−1399.
(34) Ceriotti, L.; de Rooij, N. F.; Verpoorte, E. *Anal. Chem.* **2002**, *74*, 639−647.

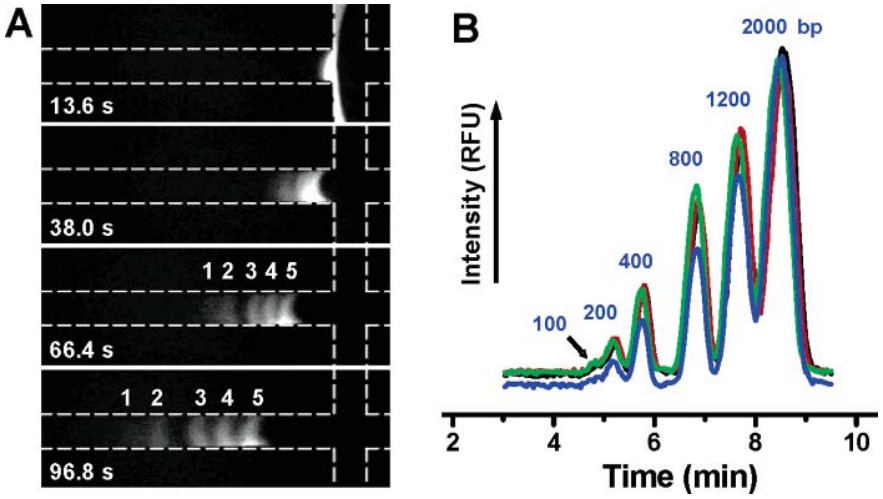

Figure 2. (A) Sequence of fluorescent images of the electrophoretic separation (15 V/cm) of a low DNA mass ladder in a microfluidic chip packed with 0.9-μm silica beads. In this case, the microchip has ~100-μm-wide and ~20-μm-deep microchannels with a cross-injection design. Dashed lines were added to aid visualization of the microchannels. Frames are time-stamped in seconds. DNA fragments 1−5 are assigned as 200, 400, 800, 1200, and 2000 bp, respectively. The 100-bp band was not detected due to the very low concentration. (B) Four consecutive runs of the same ladder obtained using 0.9-μm silica beads in a device that had been operated for ~5 h (E = 19.2 V/cm, separation length L = 5 mm).

presented in Figure 3A. The ratio of peak heights roughly corresponds to the mass ratio of DNA fragments in the ladder, allowing direct identification of individual peaks. The plate numbers were 3894−4912 for the 400-bp peak, which corresponds to plates per meter of (7.8−9.8) × 10^5 m^{-1}. This separation efficiency compares favorably with nanofabricated structures[13] and microsystems filled with gels or liquid polymer matrixes.[35−37] The 0.9-μm microsphere array effectively separates dsDNA between 100 and 2000 bp and is analogous to a 2% agarose gel, which renders pore sizes of 160−300 nm[38,39] and targets dsDNA of 0.1−3 kbp, as summarized in Table 1.

The resolution, R_s, appears to be field dependent, especially for larger DNA fragments. As the electric field decreases from 27.9 to 18.3 V/cm, R_s increases 49% (from 2.07 to 3.09) for 400−800 bp, in contrast to an increase of 146% for 1200−2000 bp (from 0.72 to 1.77). To interpret the field-dependency of DNA separations, the mechanism of size-based separation in the colloidal sieves needs to be discussed. The gyration radius of a Gaussian polymer chain is estimated by $R_g = (lL/6)^{1/2}$, where l is the Kuhn length and L the contour length.[40] R_g of 1- and 2-kbp dsDNA molecules are estimated to be ~75 and ~106 nm, respectively, slightly larger than the restrictive pores (~135 nm) in a 0.9-μm colloidal sieve. Therefore, Ogston sieving is expected as the dominant process for DNA fragments smaller than the pore size, and the crossover to the reptation regime may occur for the largest two fragments. A semilog plot of DNA mobility as a function of molecular size, shown in Figure 3B, exhibits fairly good linearity for small DNA strands, consistent with the Ogston model.[41,42] Deviation from the linear relationship was significant for 2000-bp fragment, especially under relatively high fields, which suggests a transition to the reptation regime. Figure 3C explicitly illustrates the influence of the electric field on the DNA mobility. The relative independence of the mobility of smaller DNA on the electric field further confirms the Ogston sieving mechanism, while 2000-bp DNA seems to obey the biased reptation model with fluctuations that predicts a linear dependence of mobility on field strength.[22,42]

Higher resolving power can be achieved using smaller particles to reduce the pore sizes. A mixture of a PCR marker and a low DNA mass ladder was separated using 330-nm silica beads. Ten of a total 12 peaks were identified in the separation (Figure 4A). The 100-bp peak of low abundance was blurred by the strong 50-bp peak, and the 2-kbp peak was excluded during data collection due to its very slow migration. The plates per meter for each peak were in the range of (0.2−1.4) × 10^6 m^{-1}. The resolving power was sufficient to separate two fragments with a 50-bp difference up to 800 bp (R_s = 0.89 for 750 and 800 bp), but dropped with further increasing DNA size (R_s = 0.86 for 1000 and 1200 bp), indicating the 330-nm colloidal sieve (~50-nm pore) is efficient for linear dsDNA of 50−1000 bp.

Use of this colloidal array to separate long DNA chains under constant electric fields is of great interest. Fractionation of two long DNA strands, calf thymus DNA (13 kbp) and λ-DNA (48.5 kbp), can be completed in a 0.9-μm silica sieve (~135-nm pore) within several minutes, as demonstrated in Figure 4B. This speed is comparable to that seen for a magnetically assembled colloidal post array[20] but is much faster than that seen in gel with pulsed fields. The motion of single DNA molecules was visualized (two video clips available as Supporting Information). Compared to small DNA, larger λ-DNA chains show significant elongation and experience more frequent hooking entanglement around the neck

(35) Hong, J. W.; Hosokawa, K.; Fujii, T.; Seki, M.; Endo, I. *Biotechnol. Prog.* **2001**, *17*, 958−962.
(36) Ugaz, V. M.; Lin, R.; Srivastava, N.; Burke, D. T.; Burns, M. A. *Electrophoresis* **2003**, *24*, 151−157.
(37) Emrich, C. A.; Tian, H.; Medintz, I. L.; Mathies, R. A. *Anal. Chem.* **2002**, *74*, 5076−5083.
(38) Pernodet, N.; Tinland, B.; Sturm, J.; Weill, G. *Biopolymers* **1999**, *50*, 45−59.
(39) Maaloum, M.; Tinland, B.; Weill, G. *Electrophoresis* **1998**, *19*, 1606−1610.
(40) de Gennes, P.-G. *Scalling Concepts in Polymer Physics*; Cornell University Press: Ithaca, NY, 1979.
(41) Ogston, A. G. *Trans. Faraday Soc.* **1958**, *54*, 1754−1757.
(42) Viovy, J.-L. *Rev. Mod. Phys.* **2000**, *72*, 813−872.

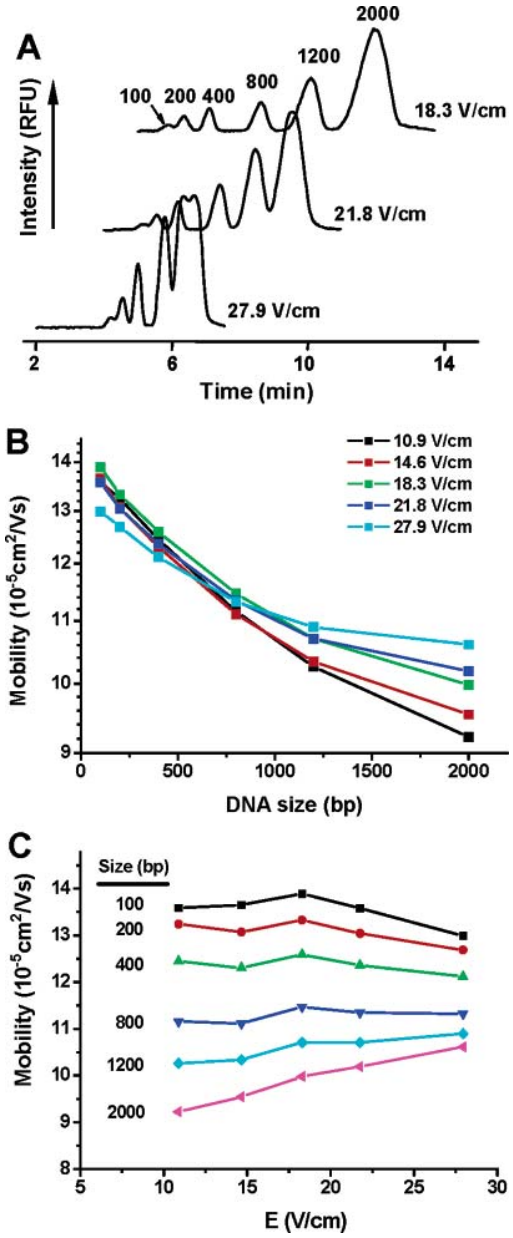

Figure 3. Influence of electric field on size separation of DNA fragments. (A) Electropherograms of a low DNA mass ladder under varied electric fields. The traces were offset for clarity. (B) Semilog plot of mobility vs DNA size at various electric fields. (C) Plot of mobility of DNA fragments of different sizes as a function of electric field. Conditions: 0.9-μm silica colloids, L = 5 mm.

between two touching spheres (seen as U-shaped elongation) during electromigration, which results in more retardation of larger λ-DNA molecules. Hooking entanglement is a well-recognized mechanism for long DNA separation in polymer matrix,[42,43] randomly dispersed gold nanoparticle/polymer composites,[44] postarrays,[5,12,20] and colloidal arrays.[23] The 0.9-μm silica array did not resolve a mixture of λ-DNA (48.5 kbp) and T4 GT7 DNA (166 kbp), whereas a 1.53-μm sphere array was able to

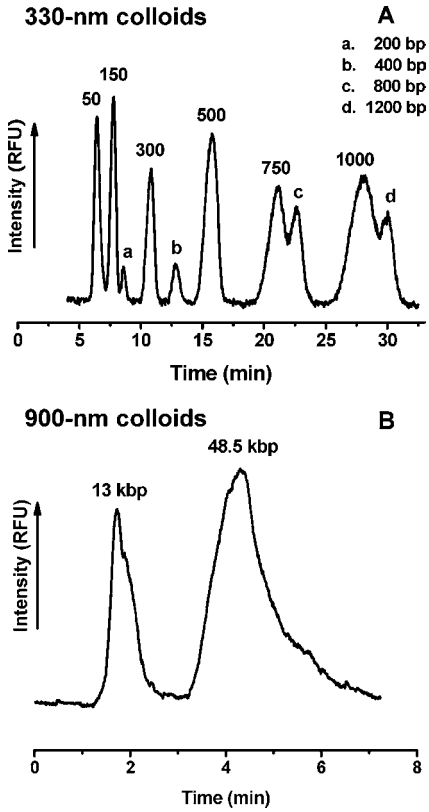

Figure 4. Separation of various dsDNA molecules using colloidal arrays of differently sized particles. (A) Electropherogram of a mixture of PCR marker (peaks marked by bp) and a low DNA mass ladder (peaks labeled a–d; the low-abundance 100-bp peak was buried by the strong 50-bp peak and the 2-kbp peak was excluded due to its long migration time) using 330-nm silica beads (E = 17.6 V/cm, L = 5 mm). A gel image of this mixture separated by slab gel electrophoresis is available to help identify all 12 fragments (Figure S-1 in Supporting Information). (B) Rapid separation of calf thymus DNA (13 kbp) and λ-DNA (48.5 kbp) within a 0.9-μm silica sphere array (E = 30 V/cm, L = 2 mm).

achieve high-speed separation of these two large molecules within 3 min in a 1.5-mm separation distance (R_s = 0.94), as evident in Figure S-2 in Supporting Information. The results demonstrate the relationship between pore size in the sphere array and the size of the molecules to be separated.

Separation of SDS-Denatured Proteins. Sieving-based protein separation in these porous beds is an obvious objective, made challenging by the very small pore size required. Figure 5 exhibits separation of SDS-denatured protein markers using differently sized silica particles. Four proteins of 20–205 kDa were separated in a matrix of 330-nm silica spheres (~50-nm pore size, E = 19.1 V/cm, L = 8 mm), as shown in Figure 5A. The resolution was 2.64 between the 20.1- and 116-kDa proteins and 3.92 between the 116- and 205-kDa proteins, respectively, which indicates a better size selectivity for larger proteins than smaller ones. Figure 5B demonstrates that the separation efficiency was greatly improved for the size range of 20–116 kDa using a 160-nm silica particle array (~24-nm pore). Five proteins were baseline resolved, despite a shorter separation distance of 4 mm (E = 30.9 V/cm).

(43) Shi, X.; Hammond, R. W.; Morris, M. D. *Anal. Chem.* **1995**, *67*, 1132–1138.
(44) Huang, M.-F.; Kuo, Y.-C.; Huang, C.-C.; Chang, H.-T. *Anal. Chem.* **2004**, *76*, 192–196.
(45) Nagata, H.; Tabuchi, M.; Hirano, K.; Baba, Y. *Electrophoresis* **2005**, *26*, 2687–2691.

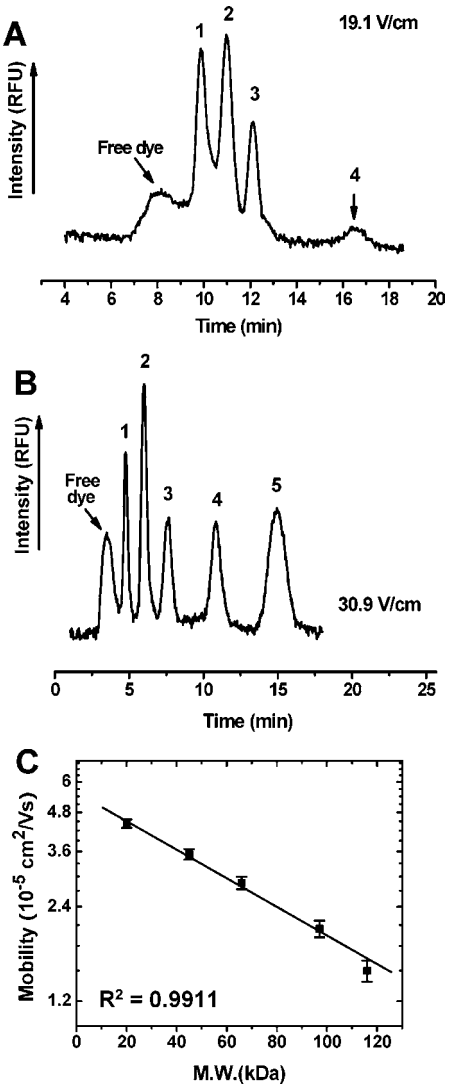

Figure 5. Separation of SDS-denatured proteins. (A) Separation of four proteins using 330-nm silica particles (E = 19.1 V/cm, L = 8 mm): (1) trypsin inhibitor, 20.1 kDa; (2) BSA, 66 kDa; (3) β-galactosidase, 116 kDa; and (4) myosin, 205 kDa. (B) Separation of five proteins using 160-nm silica particles (E = 30.9 V/cm, L = 4 mm): (1) trypsin inhibitor, 20.1 kDa; (2) ovalbumin, 45 kDa; (3) BSA, 66 kDa; (4) phosphorylase B, 97 kDa; (5) β-galactosidase, 116 kDa. A broad peak appeared before the first peak, due to the residual free dye from the labeling process. (C) A semilog plot of the apparent mobility of SDS−protein complex vs protein molecular weight with a least-squares linear fit. The averaged mobility was determined from the electrophoretic separations of five protein standards performed under the same conditions as described in (B). Error bars are standard deviation (n = 7).

This result is consistent with Ogston theory, which predicts an optimal efficiency for globular species that are close in size to the pores in the sieving matrix.[42] The plates per meter obtained using 160-nm beads were (3.3−4.5) × 10^5 m^{-1}, which corresponds to a range of plate heights of 2.2−3.0 μm, and is comparable to microfabricated nanofilter arrays[13] and microsystems using conventional gel/polymer matrixes.[2,3,45] To characterize the resolving power of the sieves, the minimum resolvable molecular weight difference was estimated using $R = \Delta M/R_s$, where ΔM and R_s denote the mass difference and the resolution between two peaks, respectively. R obtained using 160-nm beads is equal to 8.8 kDa for 66−97 and 6.2 kDa for 97−116 kDa; comparable to microsystems using gel/polymer matrixes.[3] Figure 5C shows a plot of logarithmic electrophoretic mobility against protein molecular weight. The averaged mobility for each size standard was determined from the separations (n = 7) performed under the same conditions as in Figure 5B. The relative standard deviation in mobility is less than 8% for the five standards. A linear least-squares fit to the data shows good linearity (R^2 = 0.9911), which further confirms Ogston sieving as the essential mechanism in the well-defined pores of 160-nm colloidal arrays.

CONCLUSIONS

We have demonstrated a simple microfluidic colloidal self-assembly approach for fast and economic fabrication of ordered three-dimensional molecular sieving structures into microfluidic systems. The results presented here demonstrate the flexibility of colloidal arrays in terms of the ability to precisely vary pore sizes to adjust the separation performance for a given type of biomolecule. The ability of our fabrication approach to access a wide molecular scope, ranging from proteins smaller than 10 nm to micrometer-sized long DNA coils, is challenging for conventional nanofabrication techniques, which demand sophisticated facilities and time-consuming and expensive procedures. Compared to lithographically fabricated sieving structures and microsystems using gel/polymer matrixes, the colloidal nanosieves provide comparable separation efficiency. Self-assembled colloidal array may provide an ideal system for experimentally and theoretically understanding mechanisms underlying biomolecular separation in porous media, due to the well-ordered, well-defined structure. Being compatibile with inexpensive soft lithography processing, this approach may hold the potential of commercialization for mass production of disposable size-based separation devices.

ACKNOWLEDGMENT

We thank Mei He for her assistance in SEM imaging and Eric Flaim for helping with the fabrication of PDMS chips. We thank the Nanofab at University of Alberta for the facilities and the Natural Sciences and Engineering Research Council of Canada (NSERC) for funding.

SUPPORTING INFORMATION AVAILABLE

Two video clips of electromigration of 20- and 48.5-kbp DNA under the same conditions as in Figure 4B and other additional information as noted in text. This material is available free of charge via the Internet at http://pubs.acs.org.

Received for review October 11, 2006. Accepted January 10, 2007.

AC061931H